Biophysical Journal, Volume *121*

Supplemental information

An NMR look at an engineered PET depolymerase

Cyril Charlier, Sabine Gavalda, Vinciane Borsenberger, Sophie Duquesne, Alain Marty, Vincent Tournier, and Guy Lippens

Supplementary Information for

An NMR look at an engineered PETase

Cyril Charlier, Sabine Gavalda, Vinciane Borsenberger, Sophie Duquesne, Alain Marty, Vincent Tournier & Guy Lippens

Corresponding author : Guy Lippens
Email: glippens@insa-toulouse.fr

This PDF file includes:

Tables S1 to S2

Figures S1 to S17

Residue Number	CSP (ppm)
Amide backbone (CSP > 0.1 ppm)	
192	0.188
193	0.358
196	0.160
198	0.222
211	0.113
225	0.281
226	0.285
238	0.182
239	0.498
240	0.322
241	0.138
242	0.105

Table S1 : Residues of LCC with a Ca^{2+} induced CSP > 0.1ppm

Residue Number	CSP (ppm)
Amide backbone (CSP > 0.04 ppm)	
94	0.089
97	0.053
165	0.197
167	0.064
169	0.043
188	0.041
191	0.044
194	0.061
206	0.054
207	0.078
210	0.148
212	0.422
213	0.462
217	0.043
218	0.056
237	0.057
238	0.086
241	0.051
243	0.365
244	0.080
283	0.098
285	0.051
Methyls (CSP > 0.1 ppm)	
166	0.174
212	0.296
Imidazole Histidine (CSP > 0.4 ppm)	
242	0.772

Table S2 CSP values for the different NMR probes in the titration experiment of LCC-ICC with MHET.

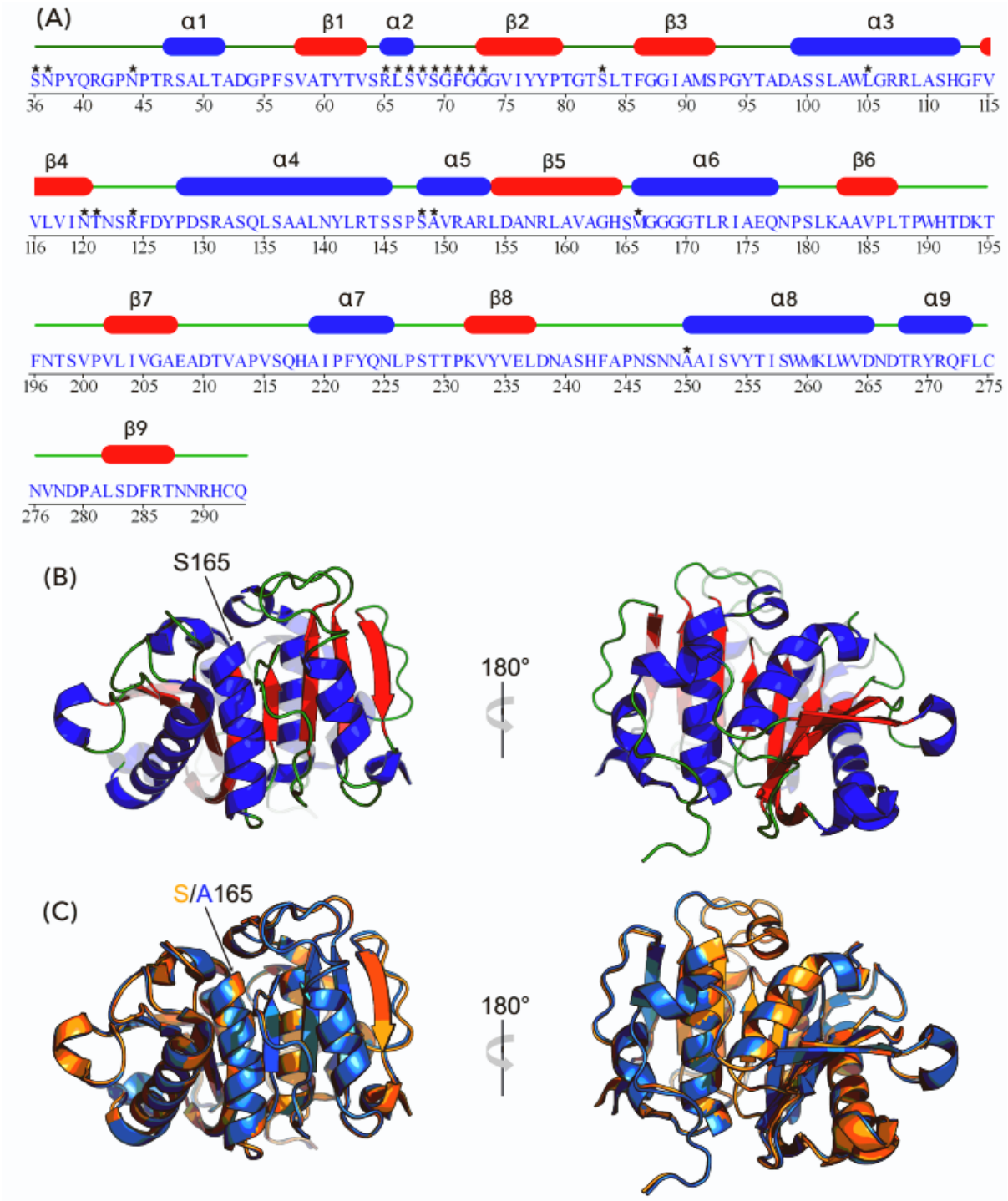

Figure S1. Structural analysis of the LCC enzyme. (A) Secondary structure elements as determined by Stride (http://webclu.bio.wzw.tum.de/stride/) with α helices in blue and β strands in red. Residues whose backbone assignment could not be obtained in this study are labeled with an * in the primary sequence. (B) 3D structure of LCC-WT (4EB0) with assigned secondary structure elements colored as in (A). (C) Overlay of LCC-WT (orange, 4EB0) and LCC-S165A (light blue, 6THS) 3D structures displaying a root mean square deviation (RMSD) over all atoms of 0.27Å. The position of the mutated residue (S165A) is indicated.

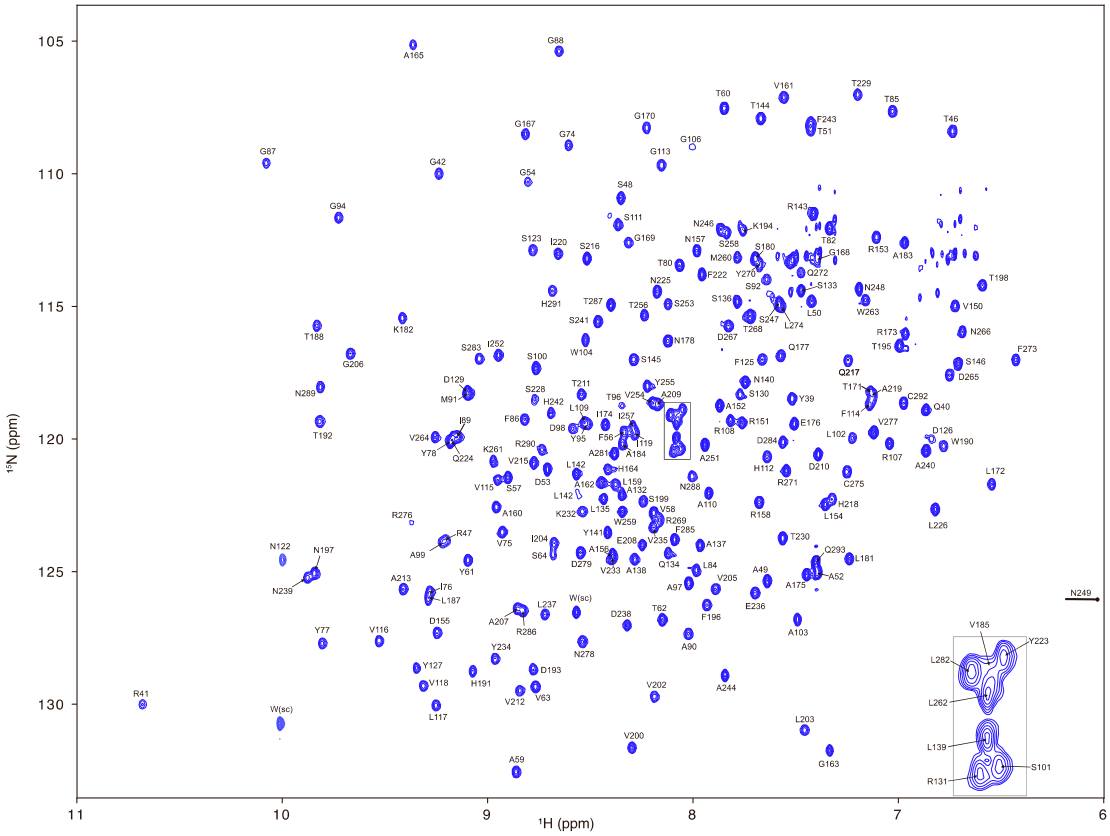

Figure S2. NMR assignment of the TROSY spectrum of LCC. 2D ^{1}H-^{15}N TROSY spectrum of LCC dissolved in 25 mM Tris-HCl buffer pH 7.5 supplemented with 100 mM NaCl. The amide proton of N249 resonates at 5.43ppm, and is outside the window shown. The resonance of A165 is folded in, and its true frequency is 135.1ppm in the nitrogen dimension. Residual signals of the Asn/Gln NH_2 groups at 6.5-7ppm/110-115ppm $^{1}H/^{15}N$ chemical shifts are not assigned.
Tryptophan side chain HN correlations are labeled as W (sc).

```
LCC         ----------------------------------------------S36NPYQRGPNPT46
Cut190      ----------------------------------------------D46NPYERGPDPT56
Tfcut2      ----------------------------------------------A1 NPYERGPNPT11

LCC         R47SALTA-DGPFSVATYTVSRLSVSGFGGGVIYYPTGTSL-TFGGIAMSPGYTADASSLAW104
Cut190      E57DSIEAIRGPFSVATERVSSF-ASGFGGGTIYYPRETDEGTFGAVAVAPGFTASQGSMSW115
Tfcut2      D12ALLEARSGPFSVSEENVSRLSASGFGGGTIYYPRENN—-TYGAVAISPGYTGTEASIAW69

LCC         L105GRRLASHGFVVLVINTNSRFDYPDSRASQLSAALNYLRTSSPSAVRARLDANRLAVAGH164
Cut190      Y116GERVASQGFIVFTIDTNTRLDQPGQRGRQLLAALDYLVERSDRKVRERLDPNRLAVMGH175
Tfcut2      L70GERIASHGFVVITIDTITTLDQPDSRAEQLNAALNHMINRASSTVRSRIDSSRLAVMGH129

LCC         S165MGGGGTLRIAEQNPSLKAAVPLTPWHTDKTF-NTSVPVLIVGAEADTVAPVSQHAIPFY223
Cut190      S176MGGGGSLEATVMRPSLKASIPLTPWNLDKTWGQVQVPTFIIGAELDTIAPVRTHAKPFY235
Tfcut2      S130MGGGGSLRLASQRPDLKAAIPLTPWHLNKNWSSVTVPTLIIGADLDTIAPVATHAKPFY189

LCC         Q224NLPSTTPKVYVELDNASHFAPNSNNAAISVYTISWMKLWVDNDTRYRQFLC-NVNDPAL282
Cut190      E236SLPSSLPKAYMELDGATHFAPNIPNTTIAKYVISWLKRFVDEDTRYSQFLCPNPTDRAI295
Tfcut2      N190SLPSSISKAYLELDGATHFAPNIPNKIIGKYSVAWLKRFVDNDTRYTQFLCPGPRDGLF249

LCC         -----S283DFR-TNNRHCQ293----------------------
Cut190      -----E296EYRSTCPYKLN305---------------------
Tfcut2      G250EVEEYRSTCPFYPNSSSVDKLAAALEHHHHHH287
```

Figure S3. Primary sequence alignment of different PETases. CLUSTAL multiple sequence alignment of the LCC sequence (Uniprot G9BY57 ; PDB ID : 4EB0) with those of Cut190 (Uniprot W0TJ64 ; PDB ID : 5ZNO) and Tfcut2 (Uniprot E5BBQ3 ; PDB ID: 4CG1). Numbering follows that of the PDB files. Residues composing the catalytic triad (Ser, Asp and His) are indicated in magenta. Calcium binding site 1 as defined in Cut190 is indicated in dark blue, Calcium binding sites 2 and 3 in light blue and green respectively. The latter two sites in LCC as confirmed by the NMR titration experiment are underlined. The A97-D98 dipeptide in LCC and its equivalent G62-T63 in Tfcut2 are shaded in grey.

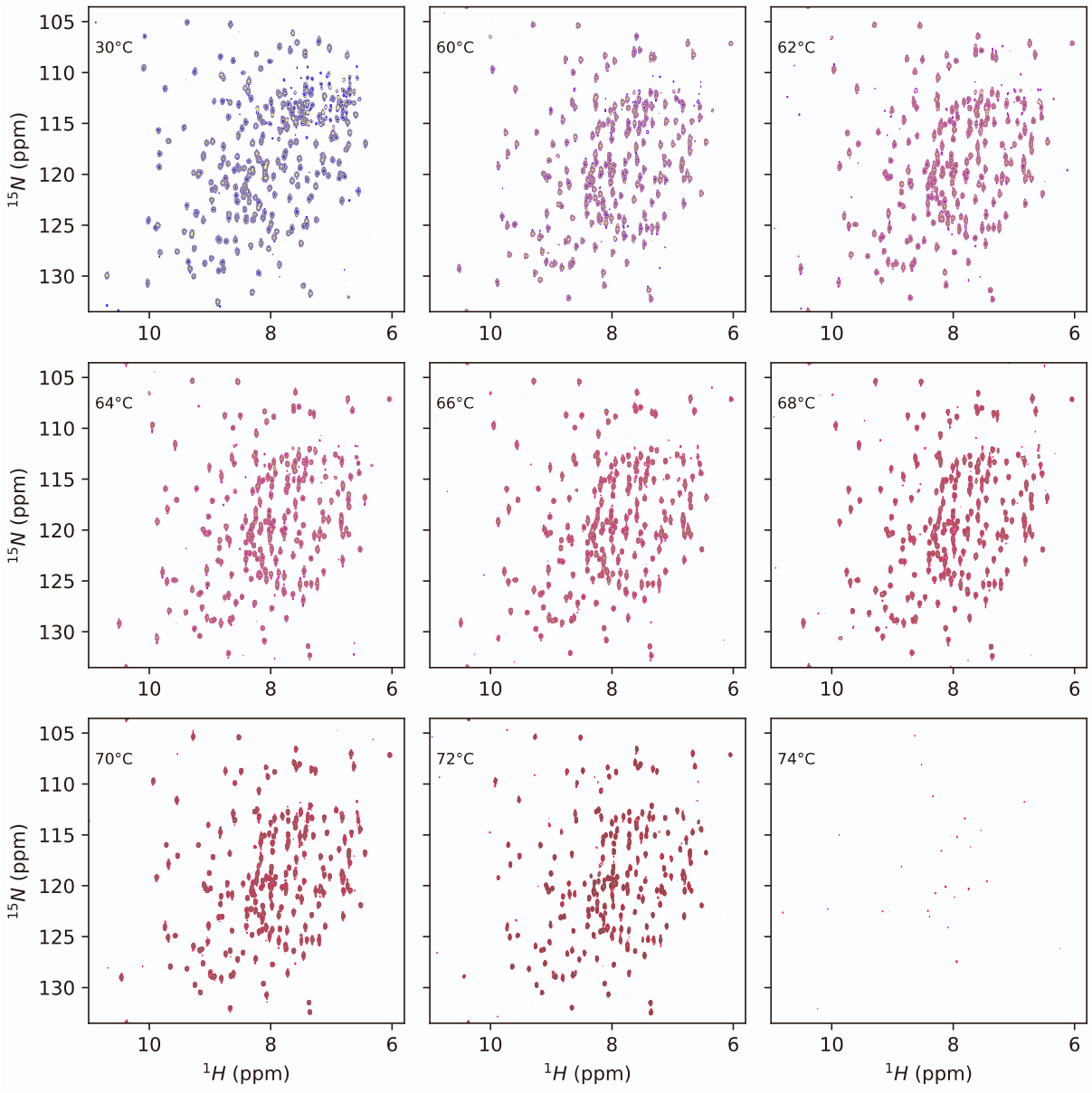

<u>Figure S4.</u> ^{1}H-^{15}N TROSY spectra of LCC as function of temperature from 30ºC up to 74ºC.

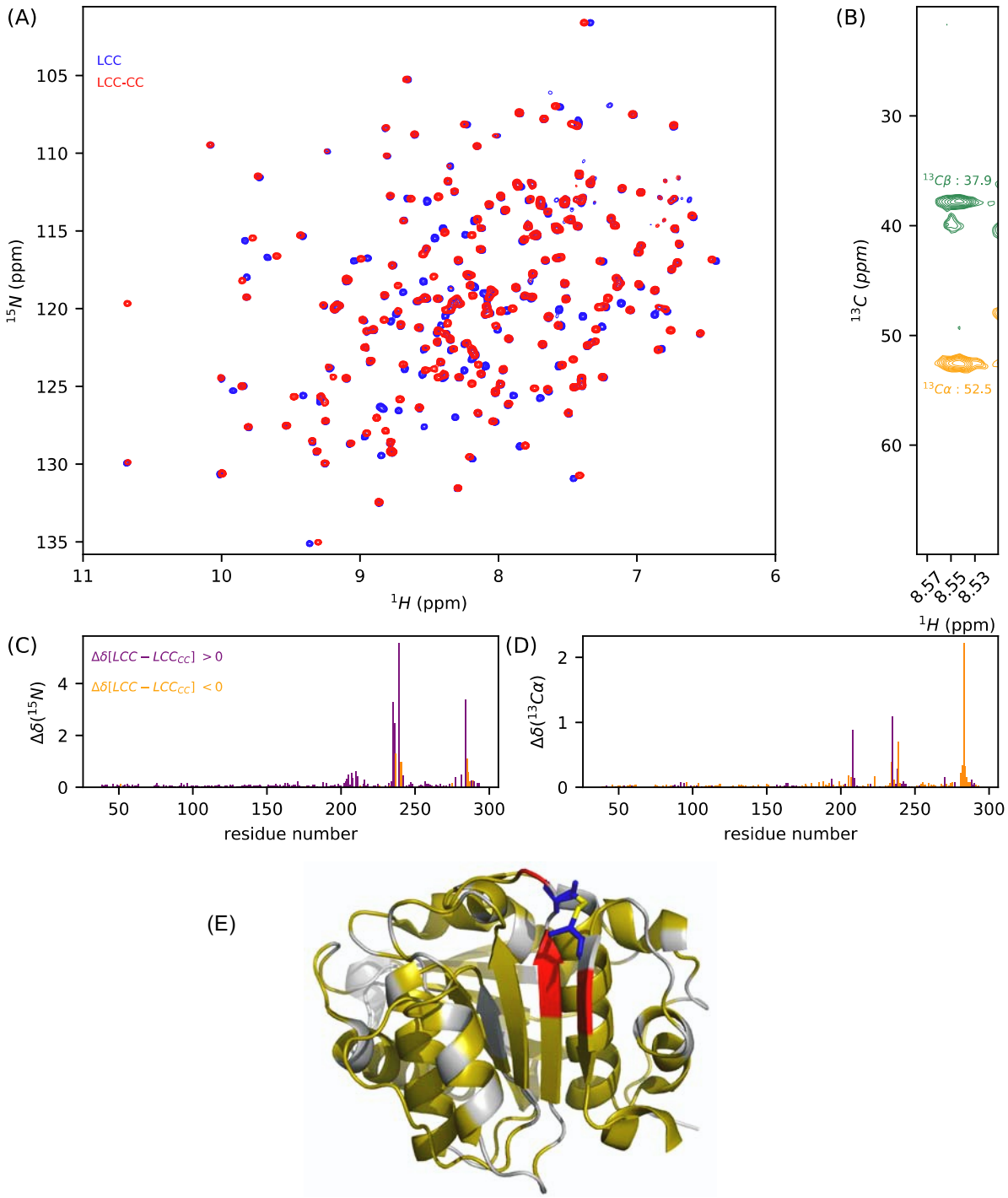

<u>Figure S5.</u> Introducing a C238-C283 disulfide bond in LCC does not change its overall structure. (A) Overlay of ^{1}H-^{15}N spectra of LCC (blue) and LCC-CC (red) recorded at 30ºC. (B) ^{1}H-^{13}C strip extracted for C238 from the HNCACB experiment of LCC-CC. Orange and green indicate positive and negative contours, respectively. Comparison of (C) ^{15}N and (D) ^{13}Cα chemical shift differences in ppm between LCC and LCC-CC. Purple and orange bars correspond to positive and negative values. (E) Mapping on the surface of LCC of the chemical shift changes (gray: no data available, yellow: 0 < $\Delta\delta$ (^{15}N) < 1, red: $\Delta\delta$ (^{15}N) > 1) induced by the D238C and S283C mutations (in blue) and ensuing disulfide bond formation (in yellow). The bond is modeled on the basis of the structure of LCC-ICCG (PDB ID: 6THT).

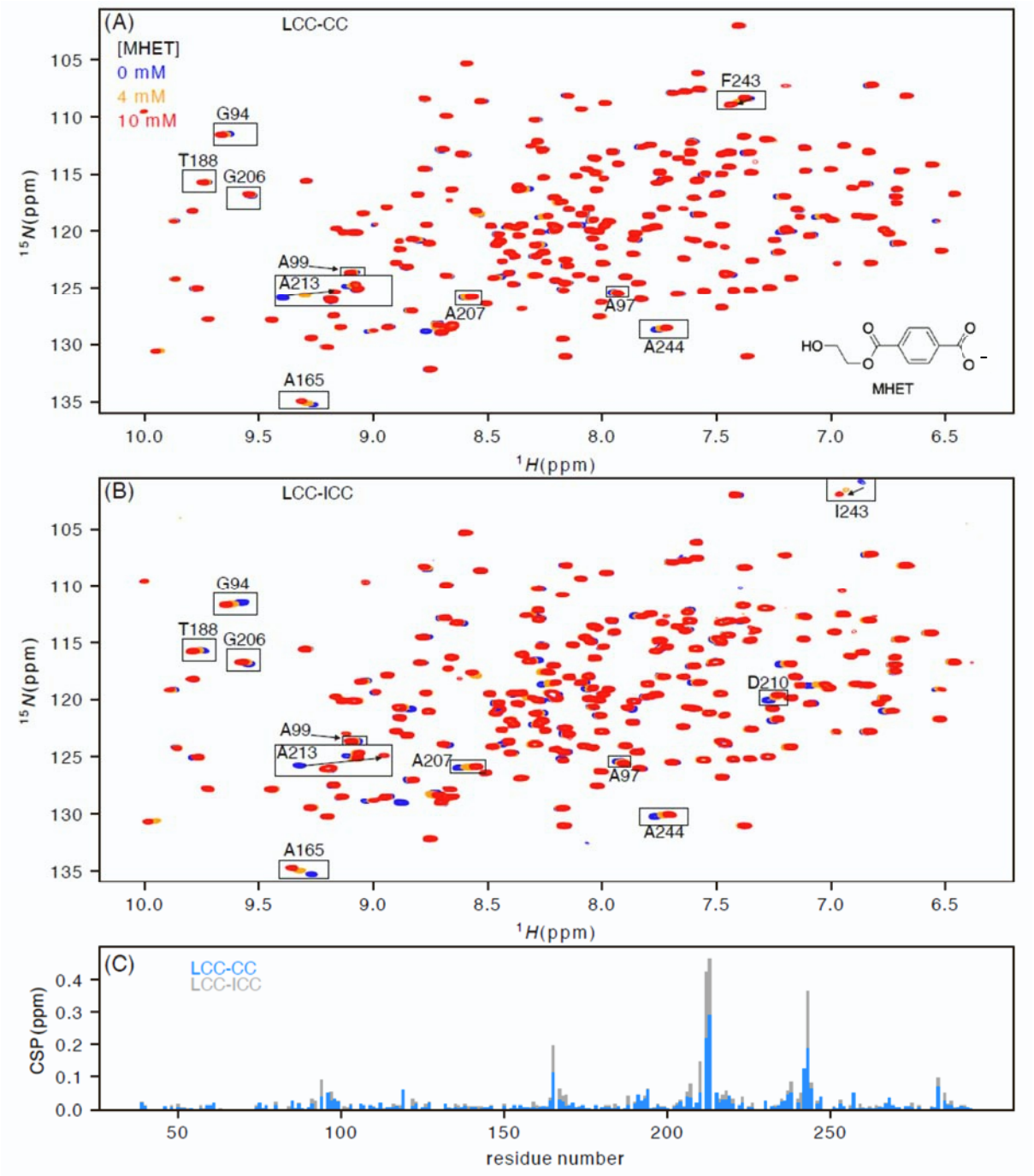

Figure S6. Mapping the molecular interactions of LCC variants with MHET. ^{1}H-^{15}N TROSY spectra of LCC-CC (A) and LCC-ICC (B) in absence (blue) and the presence of 4 mM (orange) and 10 mM (red) MHET measured at 60ºC. (C) ^{15}N/^{1}H chemical shifts perturbations induced by 10 mM of MHET in the spectrum of LCC-CC (blue) or LCC-ICC (grey).

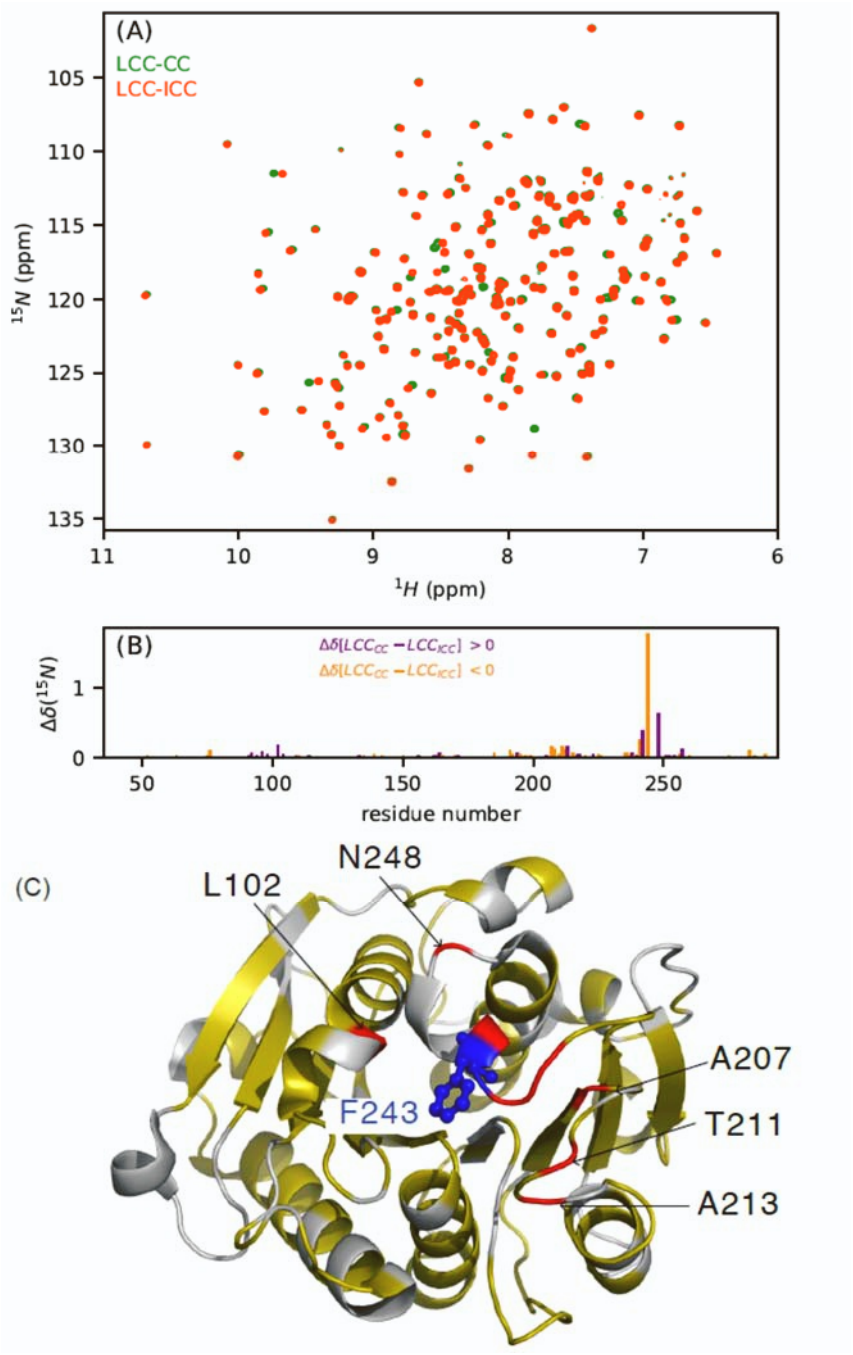

Figure S7. Impact of the F243I mutation limited to the shielding cone of the aromatic ring
(A) ^{1}H-^{15}N TROSY spectra of LCC-CC (green) and LCC-ICC (red) at 30ºC. (B) ^{15}N chemical shift differences (in ppm) between the LCC-CC and LCC-ICC. (C) ^{15}N chemical shift differences shown on the LCC structure (PDB ID: 6THS) with in gray the residues for which we have no data, in yellow residues with $0 < \Delta\delta < 0.15$ ppm and in red residue with $0.15 \text{ ppm} < \Delta\delta$. The residue F243 is shown in blue.

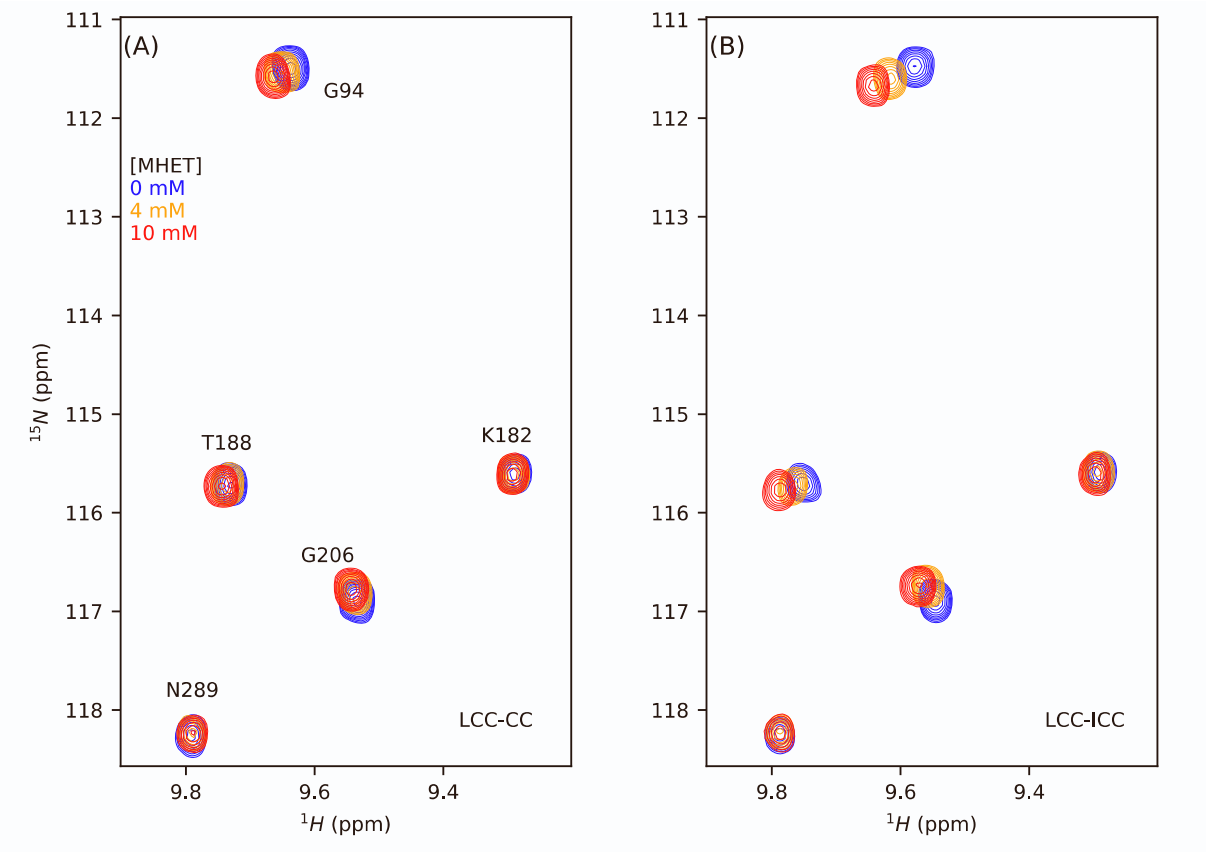

<u>Figure S8.</u> NMR mapping of MHET with the LCC mutants. Zoom of ^{1}H-^{15}N TROSY spectra of LCC-CC (A) and LCC-ICC (B) upon addition of MHET at 60ºC.

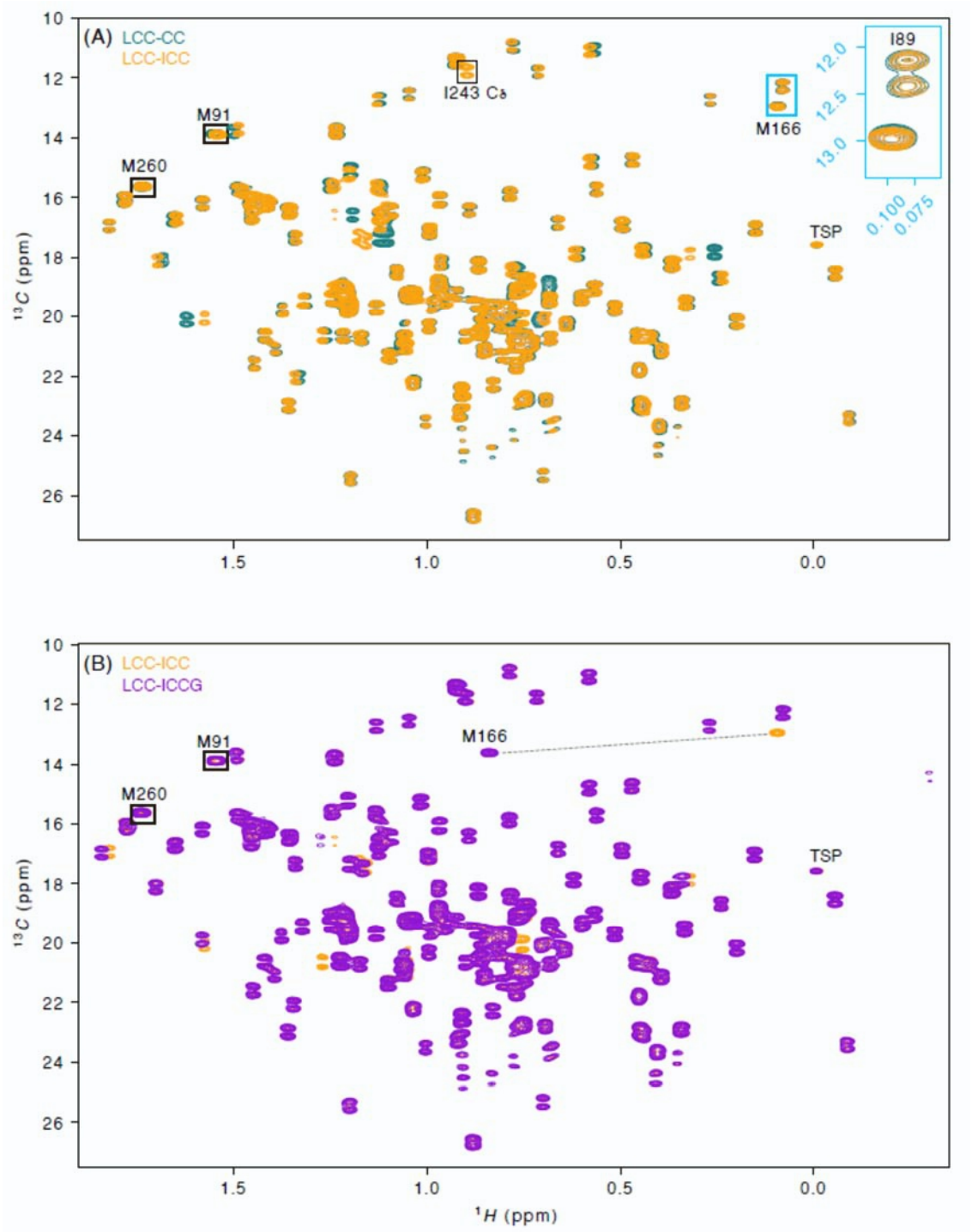

Figure S9. Methyl NMR spectra of the LCC mutants. Overlay of ^{1}H-^{13}C methyl HSQC spectra of (A) LCC-CC (teal) / LCC-ICC (orange) and (B) LCC-ICC (orange) and LCC-ICCG (purple) at 60ºC. The blue inset in (A) compares the methyl signal of M166 devoid of ^{13}C-^{13}C coupling with that of the I89 δ methyl whose carbon couples to its ^{13}Cγ nucleus.

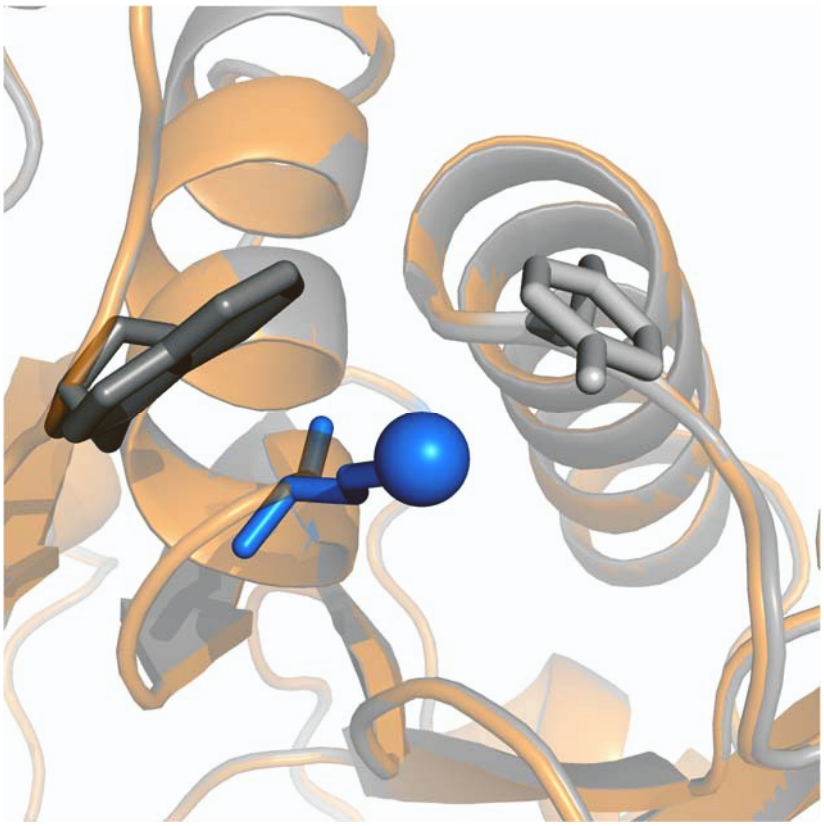

<u>Figure S10.</u> The methyl of M166 between the aromatic rings of W190 and Y127. Overlay of LCC (PDB ID: 6THS) in gray and LCC-ICCG (PDB ID: 6THT) in orange. M166 is shown in blue sticks and its methyl group as a sphere. W190 (black) and Y127 (gray sticks) from LCC are represented in sticks.

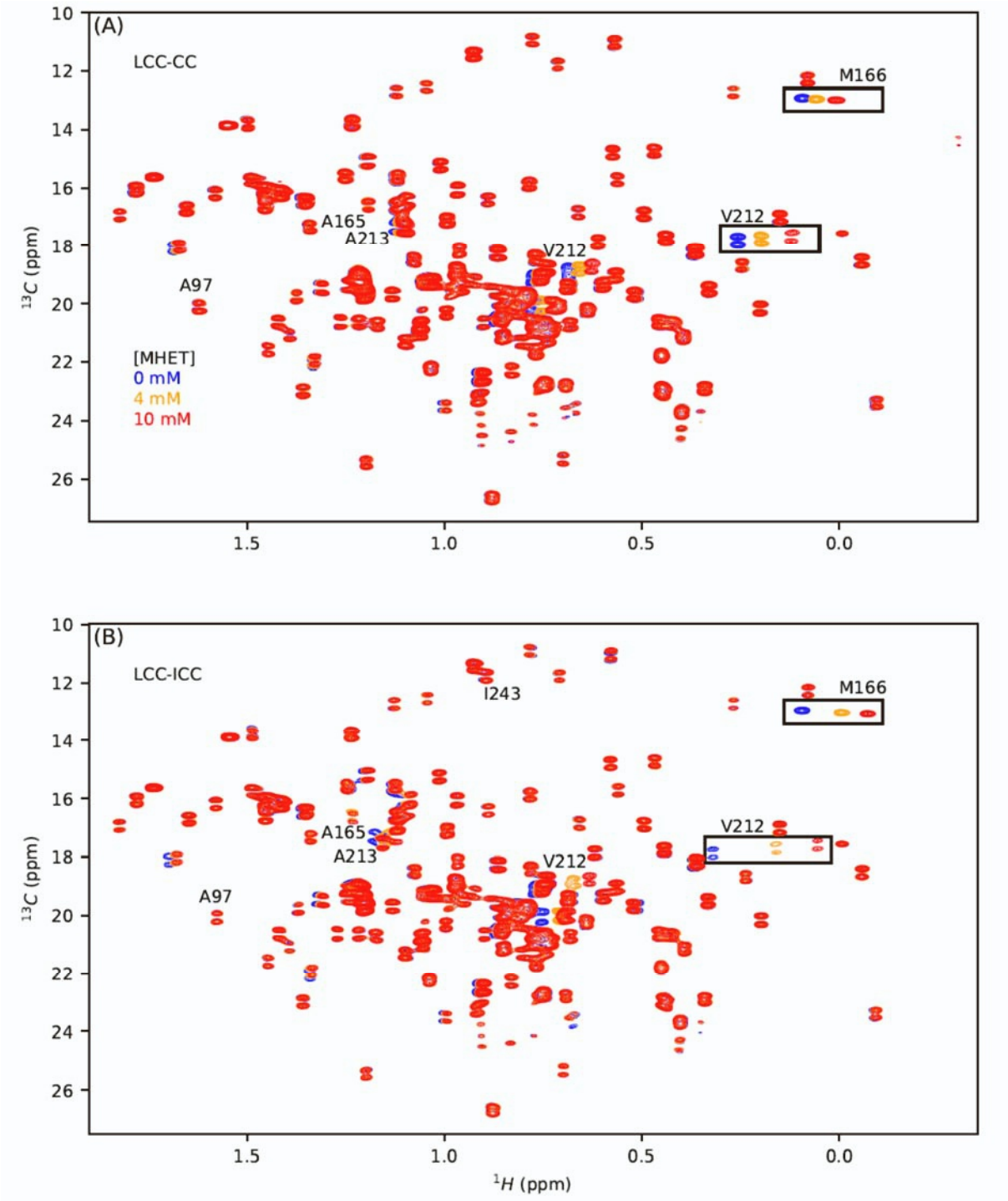

Figure S11. Methyl NMR mapping of MHET with the LCC mutants. ^{1}H-^{13}C HSQC spectra of LCC-CC (A) and LCC-ICC (B) in absence (blue) and the presence of 4 mM (orange) and 10 mM (red) MHET measured at 60ºC.

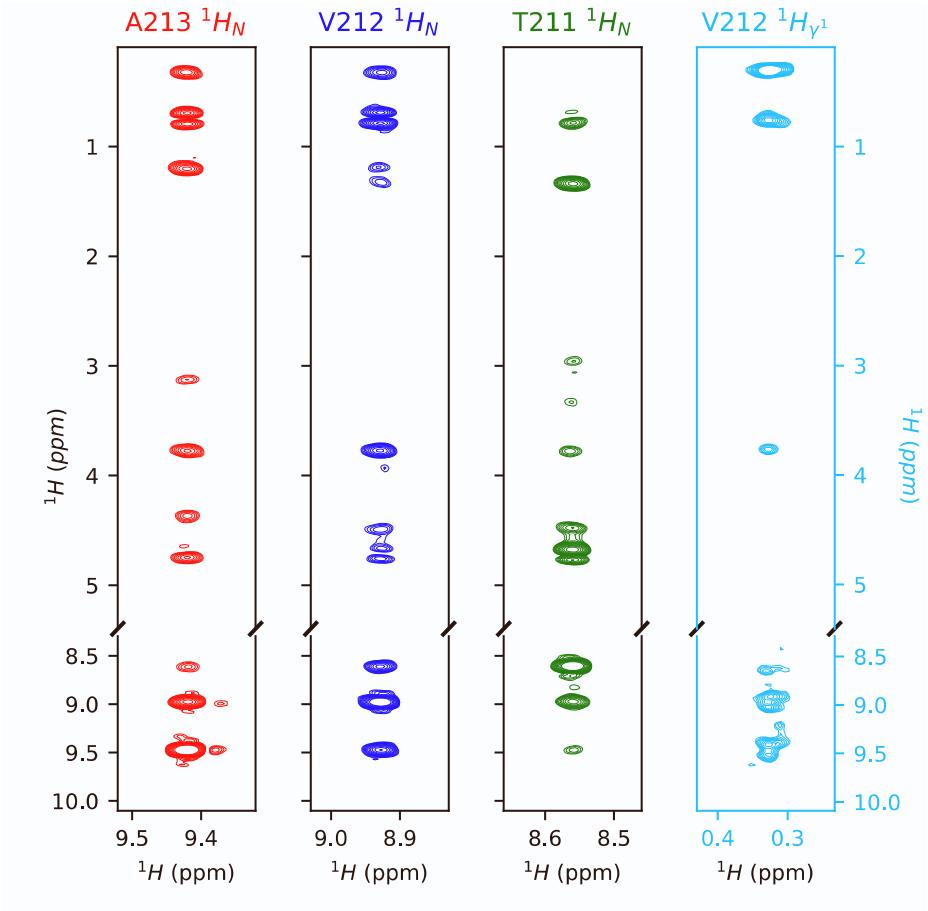

<u>Figure S12.</u> Strategy for assignment of V212 methyl groups of LCC-CC. ^{1}H-^{1}H strips from HNH-NOESY for residues T211/V212/A213. The lower parts show the correlations between amide protons, and the top parts with methyl protons. The ^{1}H-^{1}H corresponding strip for V212 in a HCH-NOESY is shown on the right side (light blue strip).

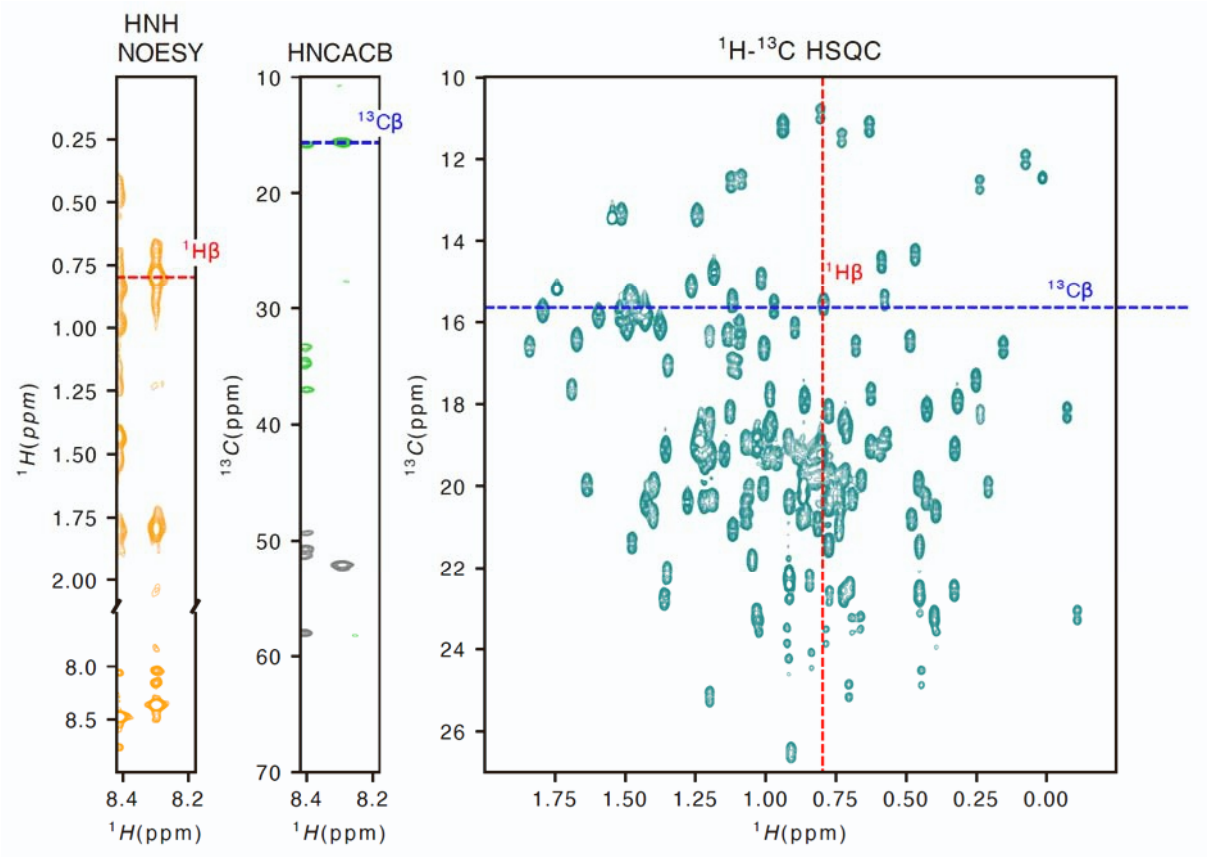

Figure S13. Strategy for assignment of Alanine methyl signals. The strip through the A138 amide correlation from the NOESY-^{1}H, ^{15}N TROSY experiment (left, orange) defines the methyl proton frequency, whereas the methyl carbon frequency can be read from the equivalent strip extracted from the HNCACB spectrum (grey for the Cα positive peak, light green for the Cβ negative peak). Both frequencies together define the position of the A138 methyl in the ^{1}H, ^{13}C HSQC spectrum (right, green).

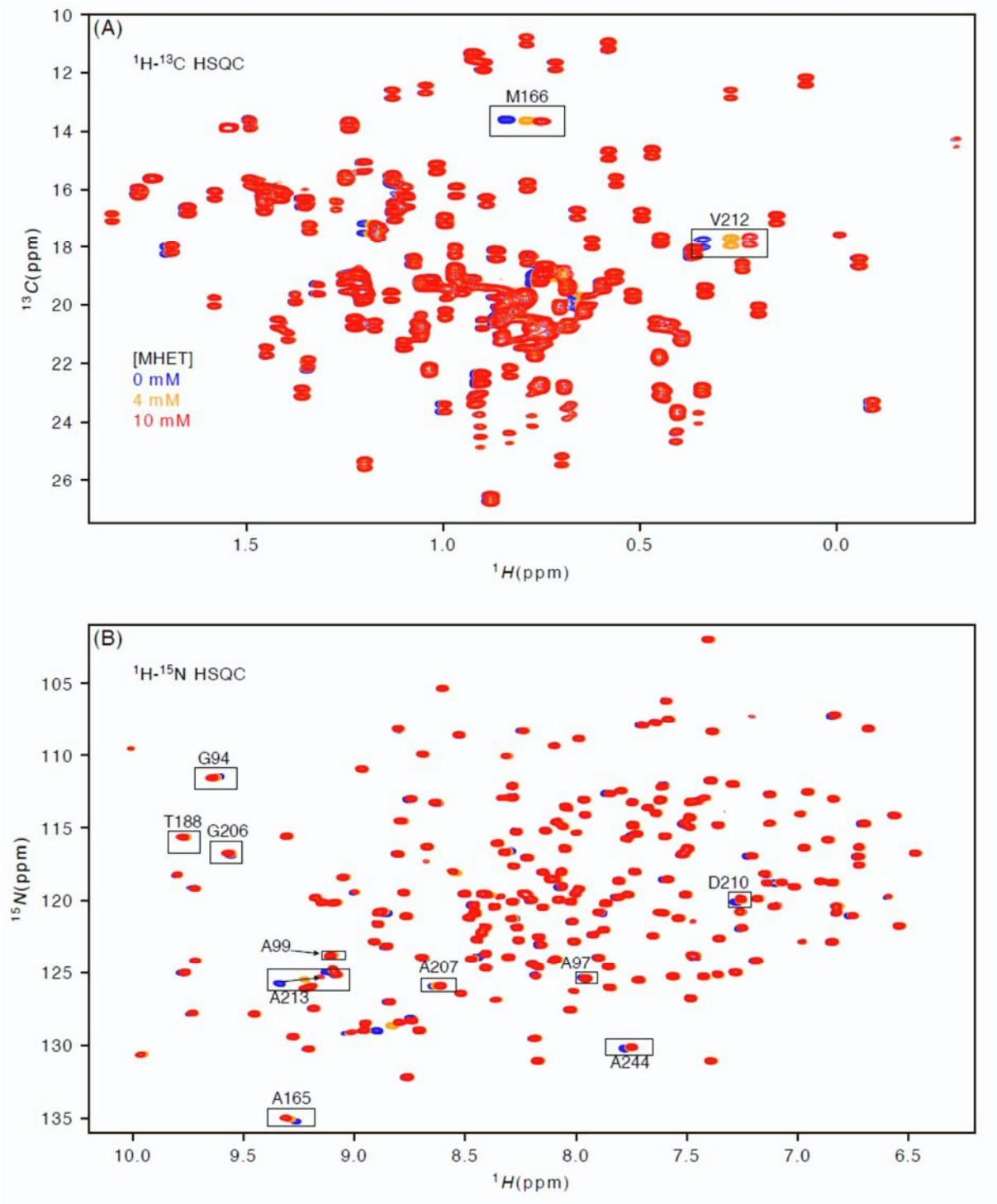

Figure S14. NMR mapping of MHET with LCC-ICCG. Interaction of LCC-ICCG with MHET reflected on ^{1}H-^{13}C HSQC spectra (A) and ^{1}H-^{15}N TROSY (B) Spectra are measured at 60ºC in absence (blue) and the presence of 4 mM (orange) and 10 mM (red) MHET.

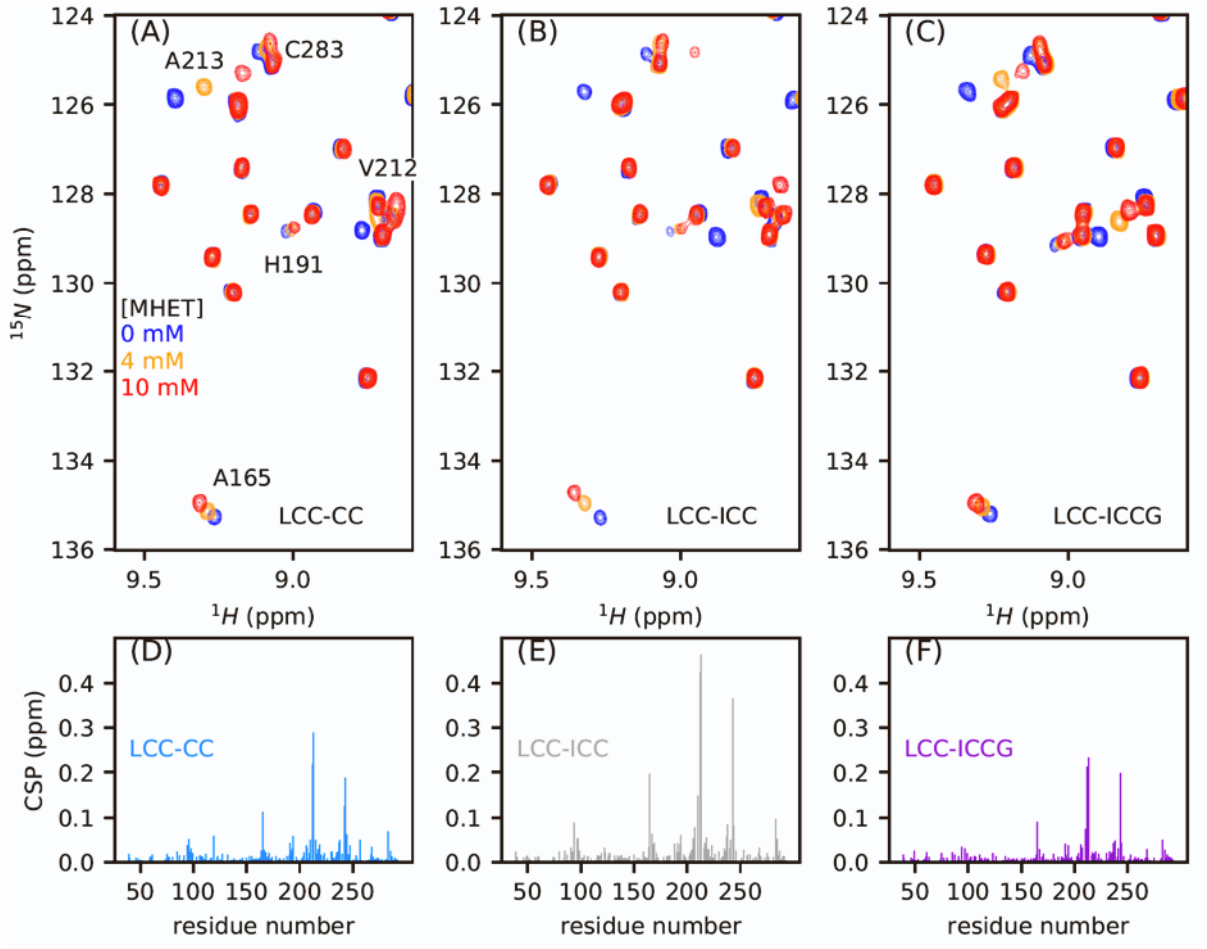

<u>Figure S15.</u> Summary of backbone NMR mapping of MHET with the LCC mutants. Interaction of MHET with LCC-CC (A, D), LCC-ICC (B, E) and LCC-ICCG (C, F). (A, B, C) Zoom on ^{1}H-^{15}N TROSY spectra in absence (blue) and the presence of 4 mM (orange) and 10 mM (red) of MHET measured at 60ºC. (D, E, F) ^{1}H-^{15}N combined chemical shift perturbations (CSPs) calculated from the spectrum in absence of MHET and in the presence of 10 mM.

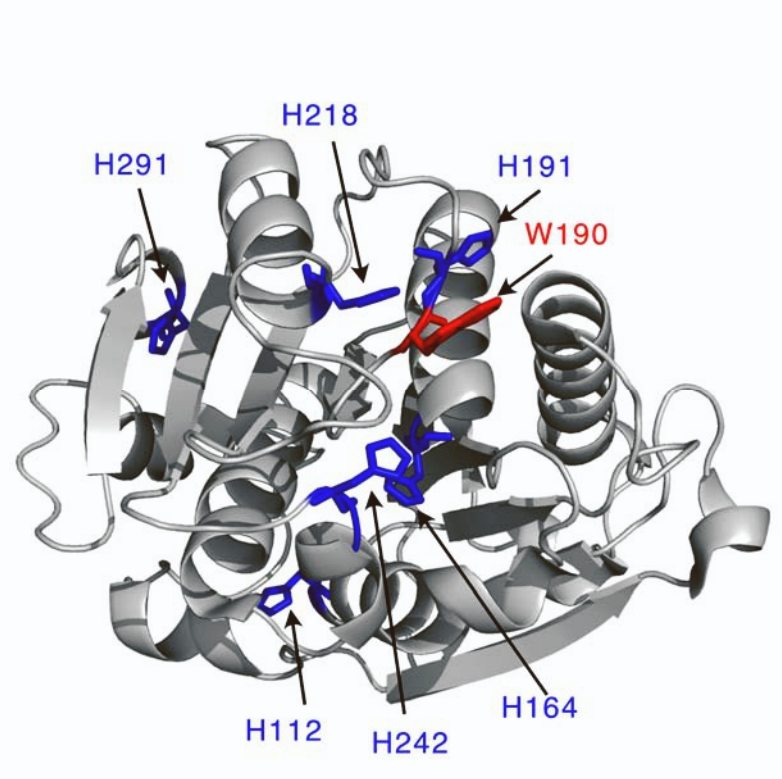

Figure S16. Histidines of LCC-ICCG. The 6 histidines of LCC-ICCG (PDB ID: 6THT) are colored in blue, W190 in red.

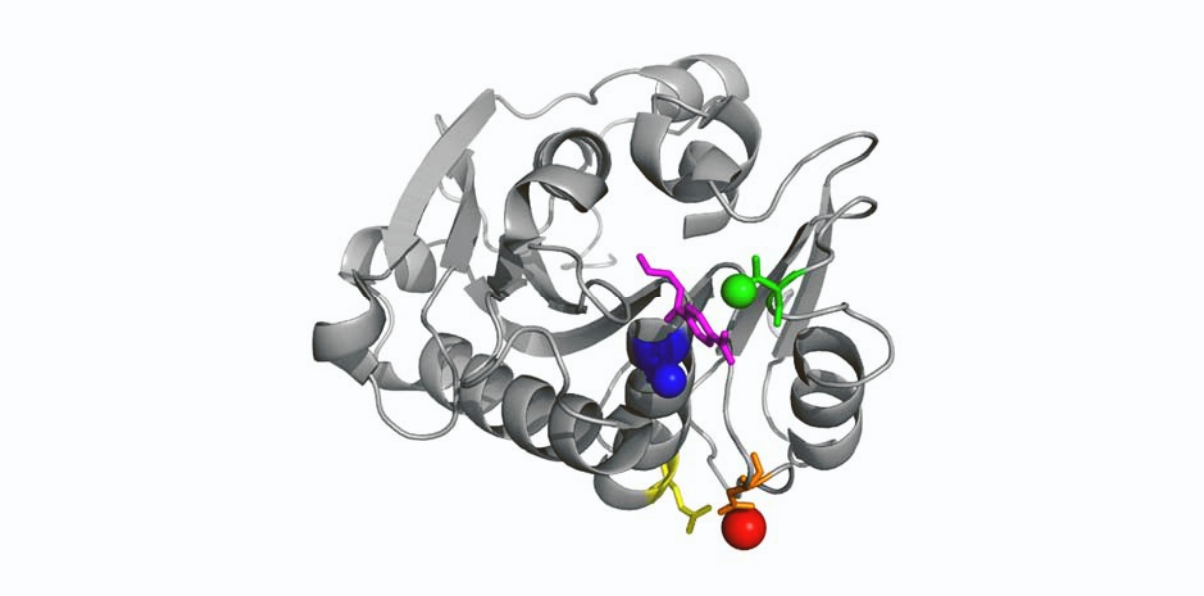

<u>Figure S17.</u> Crystal structure of LCC-ICCG in complex with MHET. The aromatic ring of the MHET moiety (in pink) is clamped between the methyls (presented as balls) of M166 (dark blue) and Val212 (green) in the recent crystal structure of the complex (PDB ID: 7VVE). A Ca^{2+} ion (red) complexed by the side chains of E176 (yellow) and D193 (orange) confirms the third binding site as defined in Cut190.